Human-mouse chimeric Fragile X syndrome model reveals FMR1-dependent neuronal phenotypes

Marine Krzisch
Whitehead Institute for Biomedical Research
Hao Wu
Fulcrum therapeutics
Bingbing Yuan
Whitehead Institute for Biomedical Research
Troy Whitfield
Whitehead Institute for Biomedical Research
Shawn Liu
Columbia University Medical Center https://orcid.org/0000-0002-2799-2519
Dongdong Fu
Whitehead Institute for Biomedical Research
Carrie Garrett-Engele
Whitehead Institute for Biomedical Research
Aaron Chang
Fulcrum therapeutics
Stephen Warren
Emory University School of Medicine
Angela Cacace
Fulcrum therapeutics
Kristin Andrykovich
Whitehead Institute for Biomedical Research
Rosalie Rietjens
Whitehead Institute for Biomedical Research
Bhav Jain
Whitehead Institute for Biomedical Research
Owen Wallace
Fulcrum therapeutics
Rudolf Jaenisch (jaenisch@wi.mit.edu)
Whitehead Institute for Biomedical Research, Cambridge, MA 02142, USA https://orcid.org/0000-0002-2540-7099

Article

Keywords: Fragile X syndrome, interspecies chimera, CGG repeats, FMRP, CRISPR/Cas9, engraftment, phenotype, single-cell sequencing

Posted Date: October 26th, 2020

DOI: https://doi.org/10.21203/rs.3.rs-83372/v1

Human-mouse chimeric Fragile X syndrome model reveals *FMR1* -dependent neuronal phenotypes

Marine A. Krzisch[1], Hao Wu[2], Bingbing Yuan[1], Troy W. Whitfield[1], X. Shawn Liu[1,5], Dongdong Fu[1], Carrie M. Garrett-Engele[1], Aaron N. Chang[2], Stephen Warren[3], Angela Cacace[2], Kristin R. Andrykovich[1], Rosalie G. J. Rietjens[1], Bhav Jain[1], Owen Wallace[2], and Rudolf Jaenisch[1,4*]*

1: Whitehead Institute for Biomedical Research, 455 Main St., Cambridge, MA, 02142

2: Fulcrum Therapeutics, 5th Floor, 26 Landsdowne St., Cambridge, MA, 02142

3: Departments of Human Genetics, Biochemistry, and Pediatrics, Emory University School of Medicine, Atlanta, GA 30322

4: Department of Biology, MIT, 31 Ames St., Cambridge, MA, 02142

5: Department of Physiology and Cellular Biophysics, Columbia University Medical Center, New York, NY 10032

*: Correspondence should be addressed to Marine Krzisch and Rudolf Jaenisch

E-mail: jaenisch@wi.mit.edu, mkrzisch@wi.mit.edu

Lead Contact: Rudolf Jaenisch jaenisch@wi.mit.edu

Keywords: Fragile X syndrome; interspecies chimera; CGG repeats; FMRP; CRISPR/Cas9; engraftment; phenotype; single-cell sequencing

Abstract

Abnormal neuronal development in Fragile X syndrome (FXS) is poorly understood. Data on FXS patients remain scarce and FXS animal models have failed to yield successful therapies. *In vitro* models do not fully recapitulate the morphology and function of human neurons. Here, we co-injected neural precursor cells (NPCs) from FXS patient-derived and corrected isogenic control induced pluripotent stem cells into the brain of neonatal immune-deprived mice. The cells populated the brain and differentiated into neurons and astrocytes. Single-cell RNA sequencing of transplanted cells revealed upregulated excitatory synaptic transmission and neuronal differentiation pathways in FXS neurons. Immunofluorescence analyses showed accelerated maturation of FXS neurons, an increased proportion of Arc-positive FXS neurons and increased dendritic protrusion width of FXS striatal medium spiny neurons. Our data show faster maturation and suggest increased synaptic activity and synaptic strength of FXS transplanted neurons. This model provides new insights into the alterations in FXS neuronal development.

Introduction

Fragile X syndrome (FXS) is characterized by physical abnormalities, anxiety, intellectual disability, hyperactivity, autistic behaviors and seizures [1]. In FXS, the expansion of the CGG triplet repeats in the *FMR1* gene leads to their hypermethylation and the hypermethylation of the *FMR1* promoter. This causes the transcriptional silencing of the *FMR1* gene after the tenth week of gestation, and the reduction or absence of *FMR1* protein (FMRP) [2]. FMRP is a RNA-binding protein and is thought to be a translational repressor at the synapse. Previous studies have suggested that its absence causes defects in neuronal development [1]. Although an imbalance of excitatory and inhibitory neuronal activity has been associated with seizure activity and autistic behaviors in several Autism Spectrum Disorders (ASDs) as well as in corresponding animal models [3-5], data on FXS patients is scarce. Morphologically, increased spine density and increased numbers of long and immature-appearing spines were found in the cortices of FXS patients, highlighting defects in neuronal connectivity in FXS [6].

So far, findings from animal models of FXS have failed to translate into successful therapies, highlighting the need to develop human cell-based models of FXS. Several research studies have used neurons derived from human induced pluripotent stem cells (iPSC) or human embryonic stem cells (ESC) cultured *in vitro* [7-10], with some studies reporting impaired maturation and synaptic hypoactivity of FXS neurons [7,8,10], and other studies showing synaptic hyperactivity and faster acquisition of synapses in FXS neurons [11,12]. Canonical two-dimensional culture conditions fail to fully recapitulate the morphological and functional characteristics of neurons in the human brain and show important intrinsic variation. Additionally, brain organoids, the most commonly used 3-dimensional *in vitro* model, contain different cell types interacting with each other, such as glial cells, neural progenitor cells and neurons, making it hard to

dissect the cell-autonomous consequences of disease-associated mutations on developing neurons, as neurons grow while interacting with cell types also affected by these mutations. Moreover, a recent study showed that stress pathways were ectopically activated in brain organoids, which impaired cell type specification. These defects were alleviated by transplantation of the organoids in the mouse brain cortex [13]. This suggests that transplantation of human neural progenitor cells (hNPCs) into the mouse brain may better reflect cellular behavior in the human brain than growth in the culture dish. Previous studies have shown that once transplanted into the neonatal brain, hNPCs migrate away from the injection site, differentiate into neurons, undergo maturation, express brain region-specific markers and become electrically active [14-16].

Here, we established a novel *in vivo* model of FXS using co-transplantation of hNPCs differentiated from FXS patient-derived iPSC and isogenic control iPSC in the brain of immune-deprived mouse neonates. We assessed the cell-autonomous effects of *FMR1* silencing on the development of human neurons in an *in vivo* context. Gene ontology analysis of single cell RNA sequencing data from transplanted FXS and isogenic control neurons showed upregulation of pathways linked to neurogenesis, neuronal differentiation and synaptic activity in FXS neurons. Transplanted FXS neurons matured faster than isogenic control, and showed a persistent increase in Arc expression. Additionally, FXS striatal medium spiny neurons (MSNs) had wider dendritic synaptic protrusions at 6-7 months post-injection (PI). Our data suggest that FXS neurons transplanted in the mouse brain mature faster and are synaptically hyperactive compared to isogenic control.

Results

Differentiation and migration of hNPCs transplanted into the neonatal brain

To investigate the developmental phenotypes of FXS neurons *in vivo*, we used two different FXS/corrected isogenic control pairs. In the FXS_SW/ C1_2_SW pair, the isogenic control C1_2_SW was generated by CRISPR-mediated deletion of the CGG repeats in the FXS patient-derived male FXS_SW iPSC line [17], leading to the reactivation of the *FMR1* promoter and FMRP reexpression (deletion pair). In the dCas9-Tet1/dCas9-dTet1 pair, the FXS patient-derived male FXS2 iPSC line was targeted with a catalytically inactive Cas9 fused to Tet1, a methylcytocine dioxygenase, as previously described [11,18]. This led to the demethylation of the CGG repeats, the reactivation of the *FMR1* promoter and FMRP reexpression (dCas9-Tet1 iPSC line). To generate a control where the CGG repeats were not demethylated, the FXS2 iPSC line was targeted with a catalytically inactive Cas9 fused to a catalytically inactive Tet1 (dCas9-dTet1 iPSC line) (Suppl. Figure 1). To eliminate the potential off-target effects associated with methylation editing in our phenotypical analysis, we compared the dCas9-dTet1 iPSC line, which is expected to display an FXS phenotype, and its isogenic control dCas9-Tet1 iPSC line (demethylation pair) in all the experiments. Both the demethylation and deletion of the CGG repeats rescued FXS neuronal activity phenotypes *in vitro* [11,12].

hNPCs were generated from these iPSCs and sorted for PSA-NCAM expression using magnetic-activated cell sorting (MACS) in order to isolate hNPCs directed towards a neuronal fate. FXS and control NPCs were labeled with different reporters (GFP or tdTomato) in order to distinguish FXS cells from control cells after transplantation into the mouse brain (Figure 1A). We characterized the hNPCs using immunofluorescence. Most cells were Pax6- and Nestin-

positive: 95%±1 C1_2_SW GFP hNPC, 90%±6 FXS_SW tdT hNPC, 95%±2 dCas9-Tet1 and 91%±2 dCas9-dTet1 hNPC co-expressed Pax6 and Nestin, two hNPC markers, showing high purity of cultured hNPCs before injection (Suppl. Figure 2). In the rest of the manuscript, the FXS_SW/ C1_2_SW and dCas9-Tet1/dCas9-dTet1 pairs will be named deletion pair: control (deletion)/FXS and demethylation pair: control (demethylation)/FXS, respectively.

We co-injected hNPCs derived from FXS and isogenic control cell lines into the brain ventricles of immune-deficient mouse neonates (Figure 1A) and analyzed the brains at 1, 3 and 6 months post-injection (PI). Transplanted hNPCs migrated through the mouse brain and populated several areas including the hippocampus, cortex, striatum, thalamus, and midbrain (Figure 1B). Most of the hNPCs differentiated into doublecortin (DCX)-positive immature neurons at 1 month PI with a small proportion of hNPCs (~10%) differentiating into immature vimentin (vim)-positive astrocytes at 1 month PI (Figure 1C, D, E), as assessed by immunofluorescence staining. This is consistent with hNPCs having been sorted for PSA-NCAM expression before injection and therefore preferentially directed towards a neuronal fate. FXS and isogenic control hNPCs yielded similar fractions of immature astrocytes and immature neurons at 1 month PI (Figure 1C-E). No obvious difference in migration was detected between FXS and isogenic control. All the transplanted cells expressed human nuclei antigen as assessed by immunofluorescence, confirming their human origin (Supplementary Figure 3). In addition, ~60 to 80% of dCas9-Tet1 (control, demethylation pair) and C1_2_SW (control, deletion pair) transplanted neurons were FMRP-positive at 1, 3 and 6 months PI. In contrast, none of the FXS_SW (FXS, deletion pair) and FXS2 (FXS, demethylation pair) cells were FMRP-positive at the same timepoints. This shows that transplanted isogenic control neurons retain stable FMRP expression *in vivo* over time (Suppl. Figure 4). Additionally, the demethylation of the *FMR1* promoter was maintained in the epigenetically edited isogenic pair, and RT-qPCR of total mRNA showed robust expression of the *FMR1* gene in C1_2_SW (control, deletion pair) cells at 1 month PI (suppl Figure 4D,E).

Accelerated maturation of transplanted FXS neurons

DAPI is predominantly impermeant to live cells, which allows it to be used as a cell viability dye, DAPI-negative cells being considered viable. In order to investigate cell-autonomous gene expression phenotypes of transplanted FXS neurons, we collected GFP+DAPI- and tdT+DAPI- isogenic control and FXS viable transplanted neurons from the deletion pair by whole-brain extraction and subsequent FACS sorting and performed single-cell RNA sequencing on the cells using the 10x Genomics platform. We analyzed two different mouse brains engrafted with FXS and isogenic control hNPCs, at 1 month PI.

FXS and isogenic control cells got assigned to similar UMAP clusters, allowing us to compare FXS and isogenic cells within the same clusters (Figure 2A). Cell types corresponding to the different clusters were annotated according to the expression of known marker genes in UMAP clusters of grouped FXS and control cells (clusters C0 to C7, Figure 2B). In line with immunofluorescence data, the cells did not express markers specific for microglia, oligodendrocyte precursor cells or oligodendrocytes (data not shown). To identify the cell types corresponding to the different clusters, we used canonical marker genes and cell cycle markers (Suppl. Figure 5A,B). Cluster C7 was very small and was excluded from further analyses. Most clusters were identified as neurons, with clusters C0 and C3 being immature neurons and cluster C5 and C6 being more mature inhibitory and excitatory neurons respectively. Cluster C4 was composed of astrocytes, and clusters C1 and C2 were identified as neural progenitor cells (NPC) via expression of markers for NPC markers and proliferation. To obtain an unbiased characterization of cellular dynamic processes, we used Slingshot [19] to assign a pseudotime to each cell, representing where the cell is along developmental trajectories. The trajectory analysis showed that cells transitioned from NPCs (clusters C1-NPC 1 and C2-NPC 2) to immature neurons (cluster C0- Immature neurons) to immature excitatory neurons (cluster C3-

Immature excitatory neurons) and then to mature neurons (cluster C5- Inhibitory neurons and cluster C6- excitatory neurons) (Suppl. Figure 5C). We also performed gene list enrichment analysis using ToppGene [20], comparing the differentially expressed (DE) genes in cluster C3 and cluster C0, cluster C3 and C5, cluster C3 and C6. Neuronal differentiation pathways were upregulated in cluster C3 compared to cluster C0, and in clusters C5 and C6 compared to cluster C3, confirming the order of progression of these clusters in terms of neuronal maturation (Suppl. Figure 5D).

Gene list enrichment analysis of the differentially expressed genes between FXS and isogenic neuronal clusters (cluster C0-immature neurons, C3-immature excitatory neurons, C5-inhibitory neurons and C6-excitatory neurons) indicated the upregulation of neurogenesis, neuronal differentiation and glutamatergic synaptic transmission pathways (Figure 2C). During neuronal differentiation, neural progenitors exit the cell cycle and differentiate into neuroblasts. Gene list enrichment analysis of the differentially expressed genes in the neuronal clusters revealed downregulation of pathways involved in cell division (Figure 2D). We analyzed the proportion of FXS and isogenic control cells in each cluster, and found that the distribution of the FXS cells was shifted towards more mature clusters (Figure 2E). Together, these data suggest that FXS cells were more mature than isogenic control cells from the deletion pair at 1 month PI. In summary, these results showed upregulation of neurogenesis, neuron development and glutamatergic synaptic transmission pathways in FXS cells, suggesting increased or accelerated neuronal maturation.

In order to further investigate alterations in the maturation and synaptic activity of FXS neurons, we analyzed transplanted neurons on brain slices using immunofluorescence. Neurons underwent morphological changes suggesting maturation from 1 to 6 months PI as indicated by the dendrites of the neurons getting thicker and longer and the cell body becoming rounder

(suppl Figure 6). Additionally, at 6 months PI, some neurons in the striatum and other brain areas displayed dendritic spines and brain region-specific marker expression (suppl Figure 5), suggesting they had undergone brain region-specific differentiation and maturation. We investigated whether FXS neurons showed accelerated maturation as compared to isogenic controls using immunofluorescence on brain slices from transplanted mice. Neuroblasts initially express doublecortin (DCX), an immature neuron marker and gradually lose DCX expression and start expressing NeuN, a mature neuron marker [21]. hNPCs transplanted into the neonatal mouse brain lost DCX and acquired NeuN expression between 1 and 6 months PI (Figure 3 A-D), confirming ongoing maturation. At 6 months PI, no DCX-positive cell could be found, suggesting that transplanted neurons had undergone full maturation.

The FXS neurons analyzed were matched with FMRP-positive (FMRP+) isogenic control neurons localized in the same brain areas. The maturation stage of FXS and FMRP+ control neurons was assessed by evaluating the fraction of DCX+, DCX+/NeuN+ and NeuN+ in the total of cells staining for DCX or NeuN at 1 and 3 months PI. As no expression of DCX was detected in transplanted neurons at 6 months PI, the maturation stage at 6 months PI was assessed using Tuj1, a generic neuronal marker expressed from mid-maturation by neurons, and NeuN. We determined the percentage of Tuj1+, Tuj1+/ NeuN+ and NeuN+ neurons as compared to the total number of neurons, defined by Tuj1 and/or NeuN labeling.

At 1 month PI, the percentage of neurons labeled with DCX and/or NeuN was similar between FXS and isogenic deletion control, suggesting that there was no difference of maturation between control and FXS neurons for this pair (Figure 3A). In contrast, for the demethylation isogenic pair, less neurons were labeled with NeuN, suggesting that FXS neurons were more immature than control neurons at that stage (Figure 3B). At 3 months PI, however, for both isogenic pairs, the proportion of NeuN+ neurons was increased, indicating more advanced

maturation of FXS neurons compared to isogenic control (Figure 3C-E). At 6 months PI, virtually all cells expressing Tuj1 expressed NeuN, suggesting that FXS and control neurons had reached full maturation at this timepoint. A small but significant increase in the percentage of NeuN+ FXS cells compared to control could still be observed for the demethylation pair, in line with accelerated maturation of FXS neurons (Figure 3F,G, H, I). This indicates that FXS neurons mature faster than isogenic controls in the mouse brain. This accelerated neuronal maturation of FXS neurons was consistent across all the brain regions analyzed.

Increased synaptic activity of transplanted FXS neurons

Previous *in vitro* experiments published by our group and other groups showed that FXS neurons in both isogenic pairs were hyperexcitable in vitro [11,12]. Furthermore, our single-cell RNA sequencing analysis at 1 month PI suggested an increase in excitatory synaptic activity in FXS neurons. Arc is an immediate early gene expressed during synaptic plasticity and is commonly used as a marker of neuronal activity. In addition, Arc is a direct inhibitor of FMRP: its translation is repressed by FMRP, and FMRP absence is expected to increase Arc expression. To determine whether Arc was upregulated in FXS neurons, we used immunofluorescence on transplanted mouse brain slices to assess Arc expression in control and FXS neurons. Neurons were defined by DCX positivity at 1 month PI, as most neurons express DCX at this timepoint and by NeuN staining at 3 months and 6 months PI, as the majority of neurons express this marker at these timepoints. At 1 month PI, a higher percentage of FXS neurons from the deletion pair was Arc-positive (Arc+) compared to isogenic control (Figure 4A). No significant difference was observed for the demethylation pair, although the percentage of FXS Arc+ neurons tended to be higher than in the isogenic control (Figure 4B). At 3 and 6 months PI, FXS neurons showed increased Arc expression (Figure 4C-G), suggesting that FXS neurons were

synaptically hyperactive in vivo. No obvious differences in the effect of *FMR1* mutation on the percentage of Arc+ neurons could be observed across analyzed brain regions.

To further investigate changes in arborization complexity, excitatory synaptogenesis and synaptic activity in FXS neurons, we assessed the dendritic protrusion density and morphology of medium spiny FXS and isogenic control neurons in the striatum at 6-7 months PI. We used DARPP32 as a marker for mature medium spiny neurons (MSNs) (Suppl. Figure 7A). Control and FXS MSNs exhibited complex morphology at 6-7 months PI (Suppl. Figure 7B, C). No significant difference in dendritic arborization complexity could be detected between FXS and isogenic control (suppl Figure 7B-F). Dendritic spines generally correspond to excitatory synapses. It is commonly accepted that increased spine head size correlates with increased synaptic strength, and dendritic spines have been found to become wider after long-term potentiation [22]. We measured dendritic protrusion density and dendritic protrusion head diameter in control and FXS neurons, using automated tracing and analysis with the Imaris software. Dendritic protrusion end diameter was significantly increased in FXS MSNs for both pairs (Figure 5A-D). We classified dendritic protrusions into three categories in function of the size of their head: head size inferior or equal to 0.3 µm, head size strictly comprised between 0.3 and 0.6 µm, and head size superior or equal to 0.6 µm. For both pairs, FXS neurons had more large protrusions (head size superior or equal to 0.6 µm) and less thin protrusions (diameter strictly comprised between 0.3 and 0.6 µm) than control neurons (Figures 5A, B, E, F). No significant change in dendritic protrusion density could be detected between control and FXS neurons (Figure 5G,H). This suggests that, although excitatory synaptogenesis in FXS MSNs is unchanged, excitatory synaptic strength is increased. This is in line with increased excitatory synaptic activity in FXS neurons. Together, these results suggest increased synaptic activity, but not synaptogenesis, in FXS neurons compared to control.

Discussion

In this study, we designed a new transplantation model of FXS, that allows FXS neurons to develop in the *in vivo* context of the mouse brain. The transplanted cells were sparsely integrated in the mouse brain and surrounded by mouse cells, allowing for the assessment of their cell-autonomous developmental defects. The transplanted hNPC were sorted for high PSA-NCAM expression but not directed towards a specific neuronal subtype, and gave rise to a high number of neurons at 1 and 3 months PI. Neurons were fully mature at 6 months PI as assessed by NeuN expression, and some neurons differentiated in MSNs in the striatum, displaying complex morphology characteristic of MSNs, a high dendritic spine density, and expressing DARPP32, a marker specific to striatal MSNs.

In this study, we found accelerated maturation of FXS neurons compared to control. In agreement with our results is another study that showed accelerated maturation of ASD neurons as compared to control neurons [23]. Furthermore, genetic haploinsufficiency of SYNGAP1/Syngap1, which commonly occurs in intellectual disability, ASD and epilepsy, also leads to accelerated maturation of neocortical pyramidal cells in a mouse model [24].

FXS MSNs displayed increased dendritic protrusion head diameter compared to isogenic control, in line with the upregulation of synaptic activity pathways as assessed by single-cell RNA seq and upregulation of Arc. This contradicts previous studies in a FXS mouse model, that showed dendritic protrusion elongation and no change in dendritic protrusion head diameter in MSNs [25]. Similarly, dendritic spine analysis in FXS patients showed increased spine density and increase in the proportion of spines with an immature morphology, i.e. with a longer neck and smaller head, in neocortical pyramidal cells [6]. This discrepancy may be explained by the fact that the dendritic spine phenotype these studies reported was non-cell autonomous and likely

caused by FXS astrocytes. Indeed, our transplanted FXS and control neurons were exposed to the same neurodevelopmental niche and FXS neurons were not in direct contact with FXS astrocytes, whereas in these two studies both neurons and astrocytes were mutant for *FMR1.* In line with this hypothesis, adult astrocyte-specific *FMR1* KO mice displayed increased spine density and a higher proportion of thin spines in the motor cortex, indicating that FXS astrocytes are necessary and sufficient for the dendritic spine phenotype of neurons in FXS [26].

Our data on Arc expression and dendritic protrusion diameter suggest that FXS neurons are hyperactive compared to control. This is in line with previous work indicating that the excitation/inhibition balance is altered in FXS patients, and suggests that cell-autonomous effects are involved in the hyperexcitability of the neuronal networks. These results are in line with previous studies from our laboratory and others [11,12] that revealed hyperexcitability in cultured FXS neurons induced by overexpression of Neurogenin-2 compared to isogenic control. Interestingly, neurons develop to form hyperexcitable networks in other intellectual disability and autism spectrum disorders, such as Kleefstra syndrome, Angelman syndrome and idiopathic ASD [27-30].

However, our work contradicts other *in vitro* studies that showed impaired maturation of FXS neurons and hypoexcitability [7,8,10]. It is of note that these studies did not use isogenic pairs of iPSC. Intrinsic variation between cell lines may be a confounding factor in studies using non-isogenic pairs. Notably, in our study, the two isogenic pairs did not display the same time course of maturation. The deletion pair matured more rapidly than the demethylation pair, as assessed by expression of DCX and NeuN.

Two genes of interest, OTX1 and TBX1 were strongly downregulated and upregulated, respectively, in FXS transplanted neurons at 1 month PI, as assessed by scRNA seq (Tables

S1 and S2). OTX1 is associated with autistic behavior and epilepsy, two symptoms of FXS. Additionally, OTX1 knock-down was previously shown to increase the astrocyte/neuron ratio in the developing cortex, and to maintain neural progenitors in the transient amplifying phase [31]. It is also required for the refinement of axonal projections of cortical neurons to subcortical targets [32]. This is in line with phenotypes previously described in FXS models: increased neural progenitor proliferation and aberrant axogenesis [33-36]. TBX1 is also associated with ASD and intellectual disability. In particular, TBX1 mutations leading to a gain of function were linked to intellectual disability [37,38]. This suggests that OTX1 and TBX1 may be interesting targets for rescuing the cell-autonomous phenotypes of FXS neurons.

A major challenge in drug development is assessing the ability of the molecules to pass the blood-brain barrier. Our human-mouse chimeric model provides us with a readout to test potential therapeutic molecules acting on the cell-autonomous phenotypes of neurons while accounting for their potential modifications in the organism and their ability to cross the blood-brain barrier, in contrary to 3D culture models. Additionally, neurons appear to reach full maturation at 6 months PI, and display complex arborization. However, the number of transplanted neurons decreased between 3 and 6 months PI, and transplanted neurons were sparse at 6 months PI, making the analysis at later timepoints tedious. Additionally, our approach does not allow us to control the fate of the transplanted cells, making the study of different neuronal subtypes difficult. To solve this issue, one could consider injecting hNPCs directed towards a striatal, cortical or hippocampal fate, or, as done in previous studies, cortical or striatal neurons [39-41]. A potential limitation of the neuronal injection approach is the low contribution of the cells to the mouse brain, as neurons are less resistant to stress than neural precursor cells and do not proliferate after injection.

Online Methods

Experimental Animals

The animals used for this study were NOD/SCID/gamma mice. They were kept in group housing under standard barrier, light and temperature-controlled conditions. Food and water were available *ad libitum*. Every effort was made to minimize the number of animals used and their suffering, and all experiments were performed in accordance with the Department of Comparative Medicine and Massachusetts Institute of Technology animal husbandry standards.

Induced pluripotent stem cell (iPSC) culture and Neural progenitor cell (NPC) differentiation

FXS patient-derived iPSC lines and isogenic control cell lines used in this study are listed in Table S3. iPSCs were cultured in feeder-free conditions on Geltrex (ThermoFisher Scientific, A1413302) or Matrigel coated flasks in StemFlexTM medium (ThermoFisher Scientific, A3349401). Cells were passaged using ReLeSRTM (STEMCELL Technology, 05873) and tested for mycoplasma contamination and karyotypic abnormalities.

NPCs were induced with dual SMAD inhibition using PSC Neural Induction medium (ThermoFisher Scientific, A1647801) according to the manufacturer's protocol. Briefly, when reaching ~80% confluency, iPSCs were dissociated with AccutaseTM Cell Dissociation Reagent (ThermoFisher Scientific, A1110501) at 37˚C for 5 min. Cell pellets were resuspended in medium after centrifugation and cell density was measured. To induce neural precursor cell (NPC) differentiation, single cells were plated at 2.5×10^5 /cm^2 in StemFlex^{TM} medium with 10 μM rock inhibitor (ref). 48 hours after plating, medium was changed to PSC Neural Induction

medium. The cells were fed every day. 6 days after induction, immature NPCs were purified with MACS sorting using anti-PSA/NCAM microbeads (Miltenyi Biotec, 130-092-966). NPCs were further expanded with neural progenitor cell expansion medium. For maintenance and further expansion, NPCs were cultured in STEMdiff™ Neural Progenitor Medium (STEMCELL Technologies, 05833) for up to 8-10 passages.

Lentiviral labeling of NPC

Lentiviruses carrying the expression cassette of GFP or tdTomato were produced by transfecting HEK293T cells with FUW constructs together with standard packaging vectors (pCMV-dR8.74 and pCMV-VSVG) followed by ultra-centrifugation-based concentration. NPCs were infected with these viruses. Once strong expression of GFP or tdT was visible, labeled NPC were purified by FACS sorting and amplified on Geltrex or Matrigel using STEMdiff™ Neural Progenitor Medium.

NPC transplantation

Cultured NPCs were dissociated using Accutase and resuspended in phosphate buffer saline without calcium and magnesium prior to injection, at a concentration of 105 cells/µL. Post-natal day 0 to post-natal day 3 mouse pups of either gender were manually injected with a total of 4x105 NPC dispersed over four injection sites in the lateral ventricles (two injection sites per brain hemisphere, one anterior and one posterior) using glass micropipettes.

Transplanted human cell extraction for single-cell RNA sequencing

Mice were euthanized using cervical dislocation, and the brains were extracted and dissociated using Miltenyi Adult mouse and rat Brain Dissociation Kit and the gentleMACS Octo Dissociator (ref). The cells were then resuspended in PBS + 0.5% BSA and stained with DAPI to determine viability. DAPI-negative GFP-positive and DAPI-negative tdT-positive cells were isolated using FACS sorting and immediately sent for single-cell RNA sequencing. Between 104 and 105 cells were obtained for each brain for each group (FXS and isogenic control).

Single-cell RNA sequencing and data analysis

The cells were sequenced immediately after extraction and FACS sorting. 5000 cells were targeted. Sequencing data was mapped to a reference meta-genome composed of human hg38 (GRCh38), mouse mm10 (GRCm38), GFP and tdTomato sequences using Cell Ranger (v3.0.2) according to the 10x Genomics pipeline. We used Ensembl version 97 gene annotation to assign UMIs to genes. Contamination of the samples by murine cells was very small, as 0.9%, 2.8%, 6.0% and 3.2% of total cells had more than 70% of UMIs mapped to mouse genes in control 1, control 2, FXS 1, and FXS 2 respectively. Only the cells with more than 95% of UMIs mapped to human genes were used for subsequent analysis.

Single-cell RNA-seq analysis

Seurat v3 [42] was used for quality control and analysis of the single cell RNA-seq experiment. We followed the Seurat Guided Clustering Tutorial (https://satijalab.org/seurat/pbmc3k_tutorial.html). To remove cells of low quality or with too few reads, the following cut offs were applied: "nFeature_RNA" above 1500, “nCount_RNA" less

than 40000, “percent.mt" less than 20. Because differences in cell cycle among individual cells can be an unwanted source of heterogeneity, these effects were mitigated by regressing out the difference between the G2/M and S phase scores, where the scores were based upon canonical markers of cell cycle. Cells were embedded in a k-nearest neighbors (kNN) graph, which was based on the Euclidean distance in the space of the 30 leading principal components. The quality of the cell partitions to clusters was optimized by applying the Louvain algorithm with a resolution of 0.2.

Differential gene expression in scRNA-seq

Since our experiment had a complex design with multiple paired replicates, we used Muscat (Multi-sample multi-group scRNA-seq analysis tools) [43] for differential expression analysis. Using the set of high-quality cells from Seurat, Muscat aggregated cells based on metadata such as samples, clusters and conditions, and created pseudo-bulk RNA-seq profiles using the sum of raw counts. Statistics for differentially expression were calculated with limma [44] using a paired design, and differential state analysis was performed with edgeR [45]. The genes with at least two-fold changes and adjusted p-values less than 0.05 were considered to be differentially expressed.

Trajectory

We performed lineage reconstruction and pseudotime inference with Slingshot [19]. We used dimensionality reduction produced by PCA, and NPC as a starting point. Since we didn’t know the order of developmental stage in the two NPC clusters (clusters C1-NPC 1 and C2-NPC 2), we ran each of these two clusters as a starting point. In both cases, two lineages were identified. The first lineage was from NPCs (cluster C1-NPC 1 or C2-NPC 2) to immature neurons (cluster C0- Immature neurons) to immature excitatory neurons (cluster C3- Immature

excitatory neurons) and then to mature neurons (cluster C5- Inhibitory neurons and cluster C6-excitatory neurons). The second lineage was from NPCs (cluster C1-NPC 1 or C2-NPC 2) to C4-astrocytes.

Gene list enrichment analysis

We performed gene list enrichment analysis on the DE protein-coding genes between control and FXS using ToppFun from the ToppGene suite [20,46]. The probability density function method was used to estimate p-values and a pathway significance threshold of FDR<0.05 was set. The Benjamini-Hochberg procedure was used to correct for multiple hypothesis testing."

DNA Methylation analysis

Pyro-seq of all bisulfite-converted genomic DNA samples was performed with the PyroMark Q48 Autoprep (QIAGEN) according to the manufacturer's instructions. The primers for pyro-seq of the *FMR1* promoter are listed below.

hFmr1_For	GAATTGGGATAATAGGATGTATTTGATTTT
hFmr1_Rev_Bio	CCCTCTCTCTTCAAATAACCT
hFmr1_Seq	TTTAGTTTTTTAGTTTTTTATTAAG

Immunohistochemistry and immunocytochemistry

Cells in culture were fixed using 4% PFA. For the IHC analysis of cells transplanted in the mouse brain, mice at 1, 3 or 6 months post-transplantation were perfused with 4% FPA through transcardial route. 100 µm-thick brain sagittal slices were sliced with Cryostat tissue slice instrument (Leica) after cryopreservation in 30% sucrose. Immunostainings were performed

using antibodies listed in Table S4. For analyses of Arc expression by IHC, a rabbit anti-FMRP antibody (Cell Signaling Technology 7104) was labeled with Alexa fluor 555 fluorophore using an antibody labeling kit (Thermo Fisher Scientific A20187). Images were acquired using a Zeiss LSM700 confocal microscope. Antibodies used in this study are listed in Table S2.

Neuronal imaging, tracing and morphometric analysis

Cells were identified as striatal medium spiny neurons using colocalization of DARPP32 immunofluorescence staining with the cell body.

Neuronal arborization analysis

Confocal microscopy z-stacks of control and FXS neurons were acquired with a 20x dry objective with zoom 0.6 using a Zeiss LSM 700 confocal microscope. Confocal microscopy z-stacks of neurons were converted to grayscale images with Fiji software (ref) and traced using Neuromantic neuronal tracing freeware (Darren Myat, http://www.reading.ac.uk/neuromantic) in semi-automatic mode. After tracing, Neuromantic generated a vector file recording morphometric data including the number of bifurcations, stems, cables (branches) and terminals. The vector files were exported to Excel for data analysis.

Dendritic spine morphology analysis

Confocal microscopy z-stacks of control and FXS neurons were acquired with a 40x oil objective with zoom 4 using a Zeiss LSM 700 confocal microscope. The z-stepsize was chosen so that two contiguous confocal plans overlap by 50%. Images were deconvolved using Huygens and a theoretical point-spread function. 3-dimension automated analysis of dendritic protrusion density and width was performed using the Filament Tracer function of the Imaris software (ref) using a

previously published protocol (Swanger et al Molecular Brain 2011). The maximum spine length and minimum spine end diameter were set at 5 μm and 0.215 μm

Statistical analyses of immunohistochemistry experiments

Statistical analyses were performed using GraphPad Prism (v. 8) software (GraphPad software, San Diego, California, USA, www.graphpad.com). Error bars in the figures indicate standard error of the mean (SEM). For neuronal maturation analysis, we performed a two-way repeated measures ANOVA test followed by a Šídák correction for multiple comparisons. For Arc expression analysis, we performed a paired t-test to compare the percentages of Arc+ FXS and isogenic control neurons. For dendritic spine protrusion tip diameter and density analysis, Shapiro–Wilk tests were performed on each group of data to test for distribution normality. When the distribution was not normal, the non-parametric Mann–Whitney test was applied. When the distribution was normal, the equality of variances of the groups was tested and the adequate unpaired t-test was used. For the analysis of the percentage of small, medium and large protrusions and the analysis of the number of bifurcations, cables, stems and terminals per neuron, a mixed-effects model was used, followed by a Šídák's multiple comparisons test.

Acknowledgements

We thank Patti Wisniewski, Patrick Autissier, and Hanna Aharonov from the FACS facility of Whitehead Institute for Biomedical Research for FACS, Jennifer Love from the Genomics core of Whitehead Institute for single-cell sequencing service. We thank George Bell for helpful discussions about statistics. We thank Wendy Salmon from the Keck Microscopy Facility of Whitehead Institute for her useful suggestions on confocal microscopy acquisitions. We thank Steve Warren in Emory University for providing FXS_SW isogenic iPSC lines. We thank

members of Rudolf Jaenisch lab and Fulcrum Therapeutics for discussion and suggestions on the manuscript. We thank Li-Huei Tsai and her group for providing the dissociator used for the extraction of transplanted cells.

Author Contributions

M.K., H.W., A.C. and R.J. conceived the idea for this study. M.K. and H.W. designed the experiments. M.K. interpreted the data. B.Y. and T.W.W. analyzed the single-cell sequencing data. M.K., H.W., D.F., C.N., performed the experiments. M.K., C.M.G., K.R.A, R.R. and B.J. analyzed the data. S.L. provided FXS2 and isogenic control iPSCs. S.W. provided the FXS_SW and isogenic control iPSCs. O.W. oversaw the first part of the study. M.K. and R.J. wrote the manuscript with input from all the other authors.

Competing interests statement

R.J. is a co-founder of Fate, Fulcrum, and Omega Therapeutics and an advisor to Camp4 and Dewpoint Therapeutics. H.W, A.N.C., A.C. and O.W. are full time employees of Fulcrum Therapeutics. The study was funded by Fulcrum Therapeutics and NIH grant 5R01MH104610-21 to R.J.

References

1 Hagerman, R. J. *et al.* Fragile X syndrome. *Nat Rev Dis Primers* **3**, 17065, doi:10.1038/nrdp.2017.65 (2017).

2 Dahlhaus, R. Of Men and Mice: Modeling the Fragile X Syndrome. *Front Mol Neurosci* **11**, 41, doi:10.3389/fnmol.2018.00041 (2018).

3 Frye, R. E. *et al.* Neuropathological Mechanisms of Seizures in Autism Spectrum Disorder. *Front Neurosci* **10**, 192, doi:10.3389/fnins.2016.00192 (2016).

4 Uzunova, G., Pallanti, S. & Hollander, E. Excitatory/inhibitory imbalance in autism spectrum disorders: Implications for interventions and therapeutics. *World J Biol Psychiatry* **17**, 174-186, doi:10.3109/15622975.2015.1085597 (2016).

5 Lee, E., Lee, J. & Kim, E. Excitation/Inhibition Imbalance in Animal Models of Autism Spectrum Disorders. *Biol Psychiatry* **81**, 838-847, doi:10.1016/j.biopsych.2016.05.011 (2017).

6 Irwin, S. A. *et al.* Abnormal dendritic spine characteristics in the temporal and visual cortices of patients with fragile-X syndrome: a quantitative examination. *Am J Med Genet* **98**, 161-167, doi:10.1002/1096-8628(20010115)98:2<161::aid-ajmg1025>3.0.co;2-b (2001).

7 Telias, M., Segal, M. & Ben-Yosef, D. Neural differentiation of Fragile X human Embryonic Stem Cells reveals abnormal patterns of development despite successful neurogenesis. *Dev Biol* **374**, 32-45, doi:10.1016/j.ydbio.2012.11.031 (2013).

8 Doers, M. E. *et al.* iPSC-derived forebrain neurons from FXS individuals show defects in initial neurite outgrowth. *Stem Cells Dev* **23**, 1777-1787, doi:10.1089/scd.2014.0030 (2014).

9 Halevy, T., Czech, C. & Benvenisty, N. Molecular mechanisms regulating the defects in fragile X syndrome neurons derived from human pluripotent stem cells. *Stem Cell Reports* **4**, 37-46, doi:10.1016/j.stemcr.2014.10.015 (2015).

10 Sheridan, S. D. *et al.* Epigenetic characterization of the FMR1 gene and aberrant neurodevelopment in human induced pluripotent stem cell models of fragile X syndrome. *PLoS One* **6**, e26203, doi:10.1371/journal.pone.0026203 (2011).

11 Liu, X. S. *et al.* Rescue of Fragile X Syndrome Neurons by DNA Methylation Editing of the FMR1 Gene. *Cell* **172**, 979-992 e976, doi:10.1016/j.cell.2018.01.012 (2018).

12 Graef, J. D. *et al.* Partial FMRP expression is sufficient to normalize neuronal hyperactivity in Fragile X neurons. *Eur J Neurosci* **51**, 2143-2157, doi:10.1111/ejn.14660 (2020).

13 Bhaduri, A. *et al.* Cell stress in cortical organoids impairs molecular subtype specification. *Nature* **578**, 142-148, doi:10.1038/s41586-020-1962-0 (2020).

14 Chen, C., Kim, W. Y. & Jiang, P. Humanized neuronal chimeric mouse brain generated by neonatally engrafted human iPSC-derived primitive neural progenitor cells. *JCI Insight* **1**, e88632, doi:10.1172/jci.insight.88632 (2016).

15 Reubinoff, B. E. *et al.* Neural progenitors from human embryonic stem cells. *Nat Biotechnol* **19**, 1134-1140, doi:10.1038/nbt1201-1134 (2001).

16 Zhou, F. W. *et al.* Functional integration of human neural precursor cells in mouse cortex. *PLoS One* **10**, e0120281, doi:10.1371/journal.pone.0120281 (2015).

17 Xie, N. *et al.* Reactivation of FMR1 by CRISPR/Cas9-Mediated Deletion of the Expanded CGG-Repeat of the Fragile X Chromosome. *PLoS One* **11**, e0165499, doi:10.1371/journal.pone.0165499 (2016).

18 Liu, X. S. *et al.* Editing DNA Methylation in the Mammalian Genome. *Cell* **167**, 233-247 e217, doi:10.1016/j.cell.2016.08.056 (2016).

19 Street, K. *et al.* Slingshot: cell lineage and pseudotime inference for single-cell transcriptomics. *BMC Genomics* **19**, 477, doi:10.1186/s12864-018-4772-0 (2018).
20 Kaimal, V., Bardes, E. E., Tabar, S. C., Jegga, A. G. & Aronow, B. J. ToppCluster: a multiple gene list feature analyzer for comparative enrichment clustering and network-based dissection of biological systems. *Nucleic Acids Res* **38**, W96-102, doi:10.1093/nar/gkq418 (2010).
21 Zhao, C., Deng, W. & Gage, F. H. Mechanisms and functional implications of adult neurogenesis. *Cell* **132**, 645-660, doi:10.1016/j.cell.2008.01.033 (2008).
22 Citri, A. & Malenka, R. C. Synaptic plasticity: multiple forms, functions, and mechanisms. *Neuropsychopharmacology* **33**, 18-41, doi:10.1038/sj.npp.1301559 (2008).
23 Schafer, S. T. *et al.* Pathological priming causes developmental gene network heterochronicity in autistic subject-derived neurons. *Nat Neurosci* **22**, 243-255, doi:10.1038/s41593-018-0295-x (2019).
24 Aceti, M. *et al.* Syngap1 haploinsufficiency damages a postnatal critical period of pyramidal cell structural maturation linked to cortical circuit assembly. *Biol Psychiatry* **77**, 805-815, doi:10.1016/j.biopsych.2014.08.001 (2015).
25 Neuhofer, D. *et al.* Functional and structural deficits at accumbens synapses in a mouse model of Fragile X. *Front Cell Neurosci* **9**, 100, doi:10.3389/fncel.2015.00100 (2015).
26 Hodges, J. L. *et al.* Astrocytic Contributions to Synaptic and Learning Abnormalities in a Mouse Model of Fragile X Syndrome. *Biol Psychiatry* **82**, 139-149, doi:10.1016/j.biopsych.2016.08.036 (2017).
27 Frega, M. *et al.* Neuronal network dysfunction in a model for Kleefstra syndrome mediated by enhanced NMDAR signaling. *Nat Commun* **10**, 4928, doi:10.1038/s41467-019-12947-3 (2019).
28 Sun, A. X. *et al.* Potassium channel dysfunction in human neuronal models of Angelman syndrome. *Science* **366**, 1486-1492, doi:10.1126/science.aav5386 (2019).
29 Takarae, Y. & Sweeney, J. Neural Hyperexcitability in Autism Spectrum Disorders. *Brain Sci* **7**, doi:10.3390/brainsci7100129 (2017).
30 Casanova, J. L., Conley, M. E., Seligman, S. J., Abel, L. & Notarangelo, L. D. Guidelines for genetic studies in single patients: lessons from primary immunodeficiencies. *J Exp Med* **211**, 2137-2149, doi:10.1084/jem.20140520 (2014).
31 Huang, B. *et al.* OTX1 regulates cell cycle progression of neural progenitors in the developing cerebral cortex. *J Biol Chem* **293**, 2137-2148, doi:10.1074/jbc.RA117.001249 (2018).
32 Weimann, J. M. *et al.* Cortical neurons require Otx1 for the refinement of exuberant axonal projections to subcortical targets. *Neuron* **24**, 819-831, doi:10.1016/s0896-6273(00)81030-2 (1999).
33 Luo, Y. *et al.* Fragile x mental retardation protein regulates proliferation and differentiation of adult neural stem/progenitor cells. *PLoS Genet* **6**, e1000898, doi:10.1371/journal.pgen.1000898 (2010).
34 Tessier, C. R. & Broadie, K. Drosophila fragile X mental retardation protein developmentally regulates activity-dependent axon pruning. *Development* **135**, 1547-1557, doi:10.1242/dev.015867 (2008).
35 Callan, M. A. *et al.* Fragile X protein controls neural stem cell proliferation in the Drosophila brain. *Hum Mol Genet* **19**, 3068-3079, doi:10.1093/hmg/ddq213 (2010).
36 Antar, L. N., Li, C., Zhang, H., Carroll, R. C. & Bassell, G. J. Local functions for FMRP in axon growth cone motility and activity-dependent regulation of filopodia and spine synapses. *Mol Cell Neurosci* **32**, 37-48, doi:10.1016/j.mcn.2006.02.001 (2006).
37 Zweier, C., Sticht, H., Aydin-Yaylagul, I., Campbell, C. E. & Rauch, A. Human TBX1 missense mutations cause gain of function resulting in the same phenotype as 22q11.2 deletions. *Am J Hum Genet* **80**, 510-517, doi:10.1086/511993 (2007).

38 Torres-Juan, L. *et al.* Mutations in TBX1 genocopy the 22q11.2 deletion and duplication syndromes: a new susceptibility factor for mental retardation. *Eur J Hum Genet* **15**, 658-663, doi:10.1038/sj.ejhg.5201819 (2007).
39 Linaro, D. *et al.* Xenotransplanted Human Cortical Neurons Reveal Species-Specific Development and Functional Integration into Mouse Visual Circuits. *Neuron* **104**, 972-986 e976, doi:10.1016/j.neuron.2019.10.002 (2019).
40 Xu, R. *et al.* OLIG2 Drives Abnormal Neurodevelopmental Phenotypes in Human iPSC-Based Organoid and Chimeric Mouse Models of Down Syndrome. *Cell Stem Cell* **24**, 908-926 e908, doi:10.1016/j.stem.2019.04.014 (2019).
41 Espuny-Camacho, I. *et al.* Pyramidal neurons derived from human pluripotent stem cells integrate efficiently into mouse brain circuits in vivo. *Neuron* **77**, 440-456, doi:10.1016/j.neuron.2012.12.011 (2013).
42 Stuart, T. *et al.* Comprehensive Integration of Single-Cell Data. *Cell* **177**, 1888-1902 e1821, doi:10.1016/j.cell.2019.05.031 (2019).
43 Crowell, H. L. *et al.* On the discovery of subpopulation-specific state transitions from multi-sample multi-condition single-cell RNA sequencing data. *bioRxiv*, 713412, doi:10.1101/713412 (2020).
44 Ritchie, M. E. *et al.* limma powers differential expression analyses for RNA-sequencing and microarray studies. *Nucleic Acids Res* **43**, e47, doi:10.1093/nar/gkv007 (2015).
45 McCarthy, D. J., Chen, Y. & Smyth, G. K. Differential expression analysis of multifactor RNA-Seq experiments with respect to biological variation. *Nucleic Acids Res* **40**, 4288-4297, doi:10.1093/nar/gks042 (2012).
46 Chen, J., Xu, H., Aronow, B. J. & Jegga, A. G. Improved human disease candidate gene prioritization using mouse phenotype. *BMC Bioinformatics* **8**, 392, doi:10.1186/1471-2105-8-392 (2007).

Figures

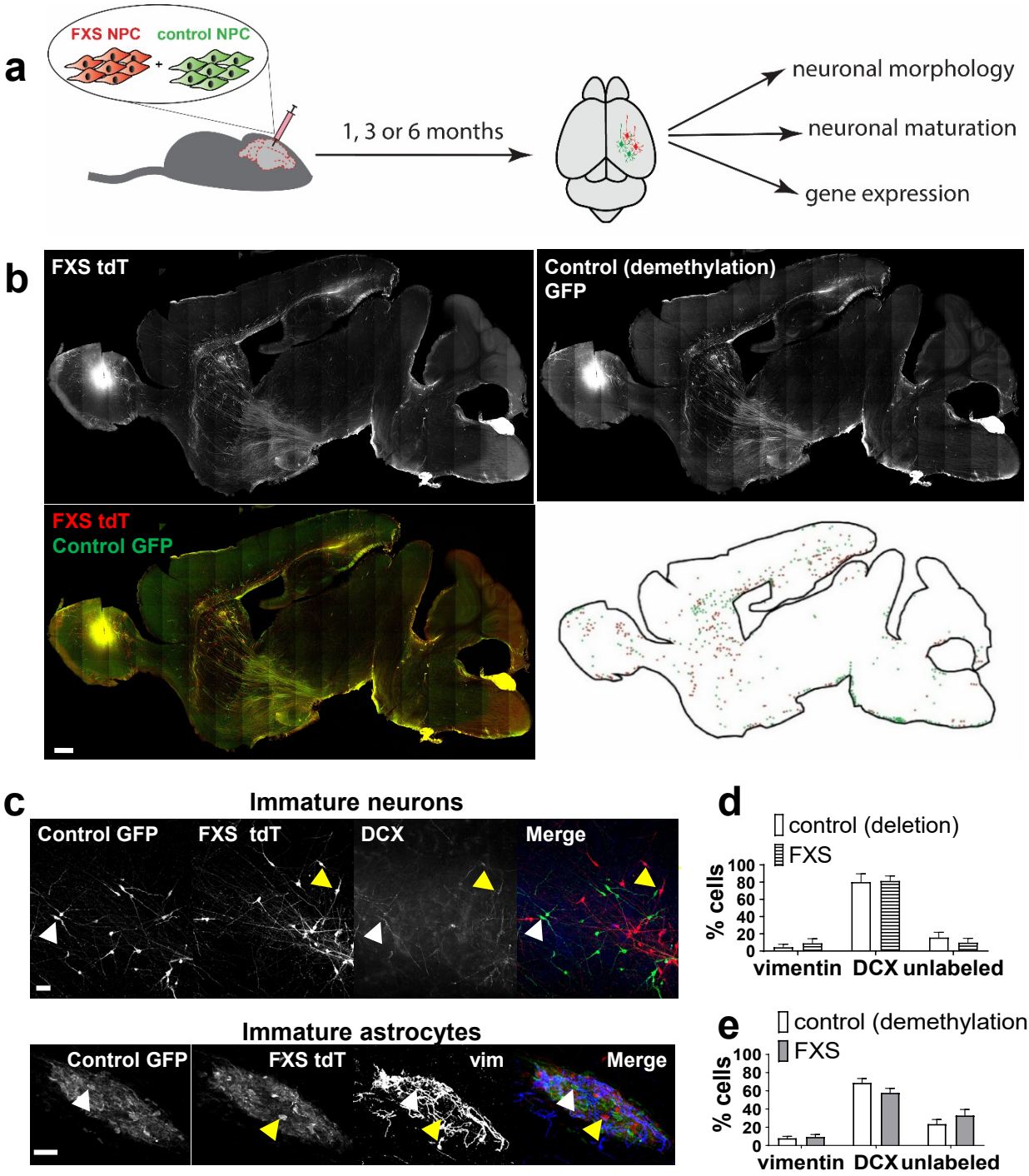

Figure 1: **Transplanted hNPCs populate several areas of the brain and differentiate into neurons and astrocytes. a.** Co-injection of FXS hNPCs labeled with tdTomato and isogenic control hNPCs labeled with GFP in the cerebral ventricles of NSG mouse neonates. Brains were harvested at 1, 3 or 6 months post-injection (PI). **b.** Maximum intensity projection of a 100 µm-thick mouse brain slice at 1 month PI. Scale bar represents 200 µm. Red: tdTomato-labeled FXS; green: GFP-labeled isogenic control (demethylation). **Right lower panel:** localization of the cell bodies of transplanted FXS (red) and isogenic control (green) cells. **c. Upper panel:** Transplanted hNPCs from FXS and isogenic control (demethylation) labeled with doublecortin (DCX) at 1 month PI. **Lower panel:** Transplanted FXS and isogenic control (demethylation) hNPCs labeled with vimentin (vim) at 1 month PI. Red: tdTomato-labeled FXS; green: GFP-labeled isogenic control. The Yellow and the white arrow show the cell body of a FXS and control cell respectively. Scale bars represent 40 µm. **d.** Percentage of FXS and isogenic control (deletion) cells labeled with vim, DCX, or unlabeled at 1 month PI. 2-way repeated measures ANOVA; N= 4 animals, 17 to 109 neurons per animal for each group. **e.** Percentage of FXS and isogenic control (demethylation) cells labeled with vim, DCX, or unlabeled at 1 month PI. 2-way repeated measures ANOVA; N= 4 animals, 118 to 140 neurons per animal for each group. Bar heights and whiskers represent the mean +/- SEM.

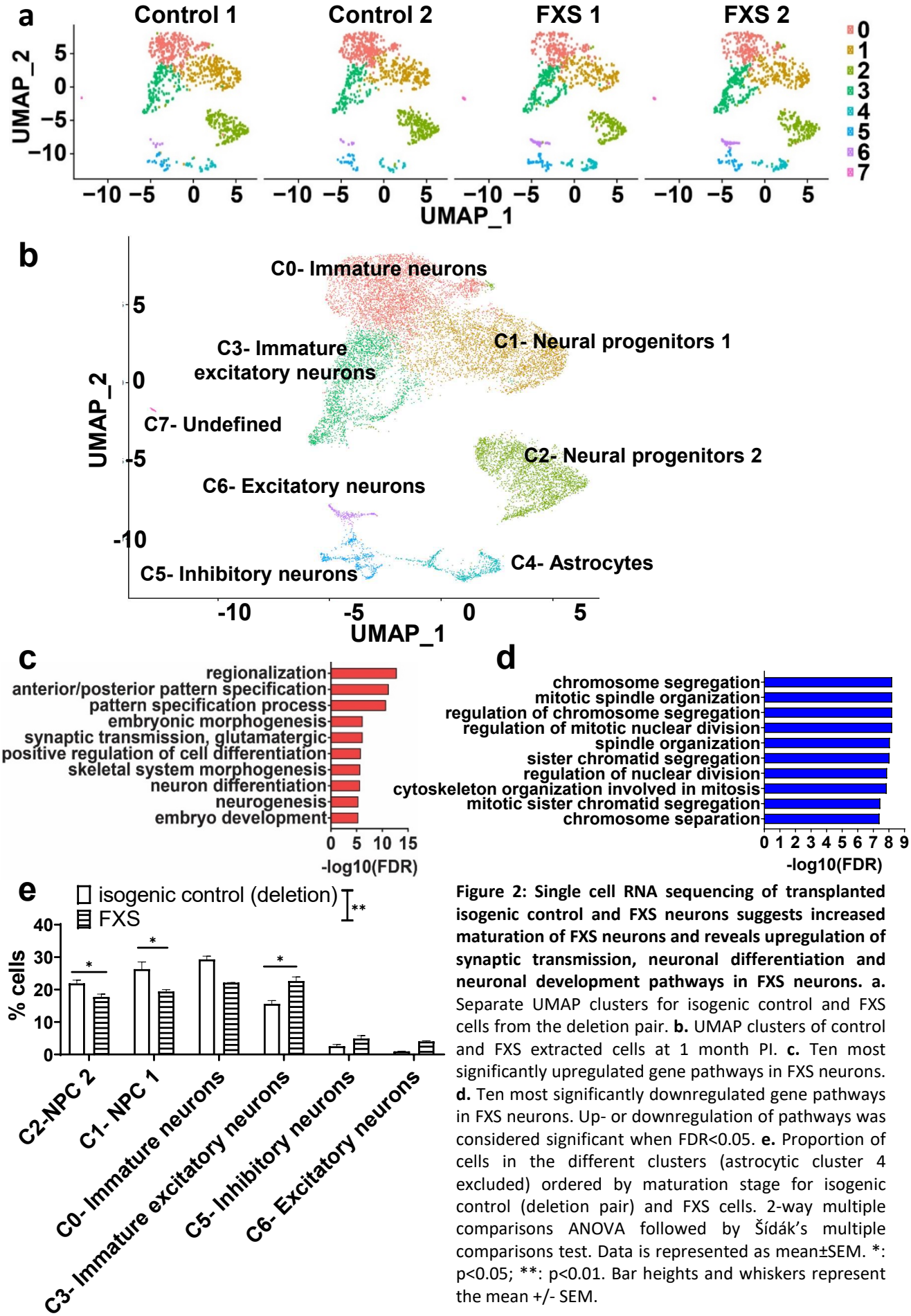

Figure 2: Single cell RNA sequencing of transplanted isogenic control and FXS neurons suggests increased maturation of FXS neurons and reveals upregulation of synaptic transmission, neuronal differentiation and neuronal development pathways in FXS neurons. a. Separate UMAP clusters for isogenic control and FXS cells from the deletion pair. **b.** UMAP clusters of control and FXS extracted cells at 1 month PI. **c.** Ten most significantly upregulated gene pathways in FXS neurons. **d.** Ten most significantly downregulated gene pathways in FXS neurons. Up- or downregulation of pathways was considered significant when FDR<0.05. **e.** Proportion of cells in the different clusters (astrocytic cluster 4 excluded) ordered by maturation stage for isogenic control (deletion pair) and FXS cells. 2-way multiple comparisons ANOVA followed by Šídák's multiple comparisons test. Data is represented as mean±SEM. *: p<0.05; **: p<0.01. Bar heights and whiskers represent the mean +/- SEM.

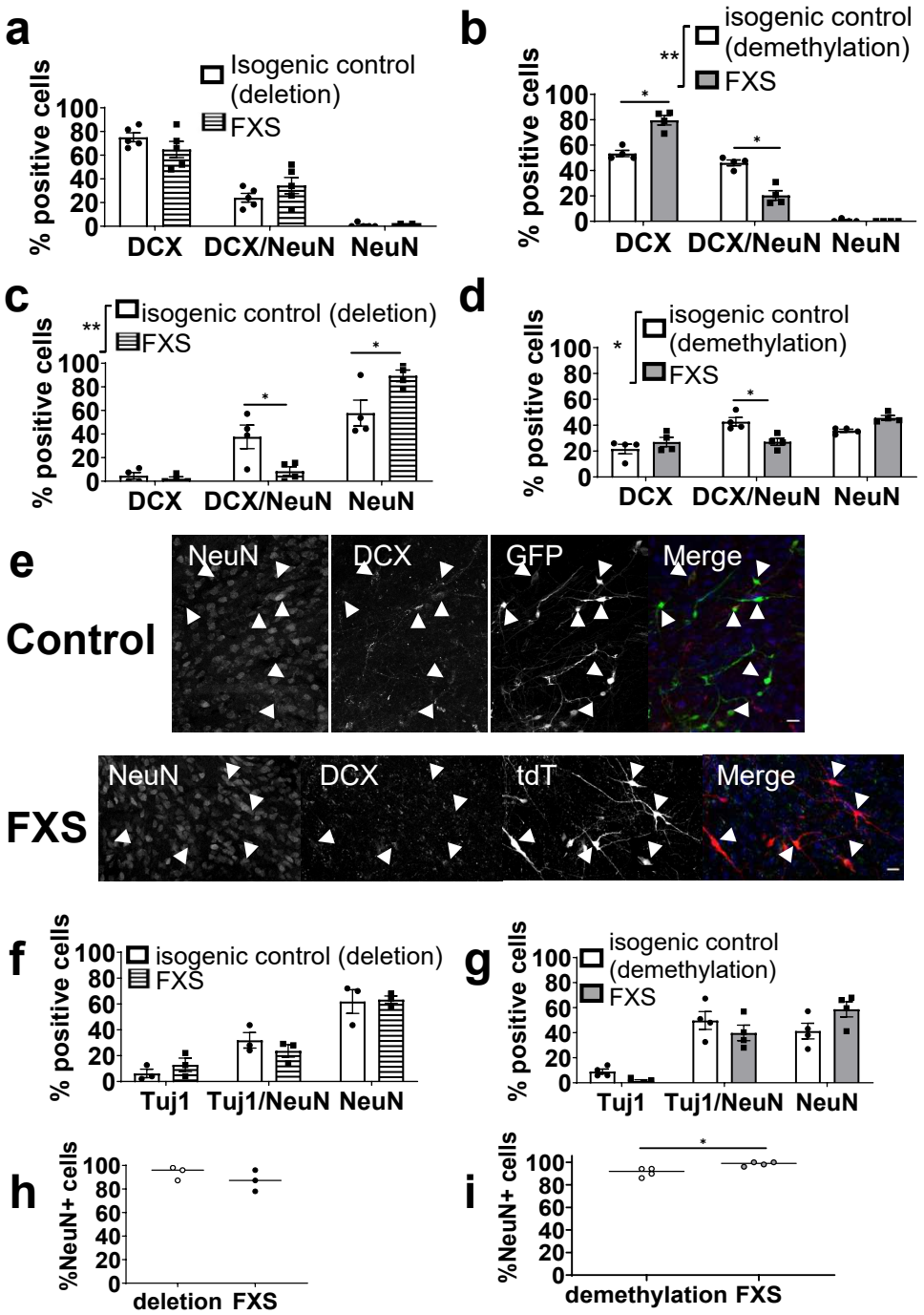

Figure 3: Transplanted FXS neurons mature faster than isogenic control. Percentage of doublecortin+ (DCX), doublecortin+ NeuN+ (DCX/NeuN) and NeuN+ (NeuN) cells at 1 month post-injection (PI) in control and FXS cells from the deletion pair (**a**) and from the demethylation pair (**b**). Repeated measures two-way ANOVA followed by Šídák's multiple comparisons test; N=4 mice, 30 to 72 neurons per mouse per group. Percentage of doublecortin+ (DCX), doublecortin+ NeuN+ (DCX/NeuN) and NeuN+ (NeuN) cells at 3 months PI in control and FXS cells from the deletion pair (**c**) and from the demethylation pair (**d**). Repeated measures two-way ANOVA followed by Šídák's multiple comparisons test; N=4 mice, 45 to 73 neurons per mouse per group. **e.** Confocal maximum intensity projection of isogenic control (deletion) (**upper panel**) and FXS (**lower panel**) neurons immunostained with doublecortin (DCX) and NeuN at 3 months PI. White arrows indicate the cell bodies of neurons. Scale bars represent 20 µm. Percentage of Tuj1+, Tuj1+ NeuN+ (Tuj1/NeuN) and NeuN+ (NeuN) cells at 6 months PI in control and FXS cells from the deletion pair (**f**) and from the demethylation pair (**g**). Repeated measures two-way ANOVA; N=3 to 4 mice, 49 to 55 neurons per mouse per group. **h.** Total percentage of NeuN+ cells at 6 months PI in control and FXS cells from the deletion pair (**h**) and from the demethylation pair (**i**). Paired t-test; N=3 to 4 mice, 49 to 55 neurons per mouse per group. *: $p<0.05$. Bar heights and whiskers represent the mean +/- SEM.

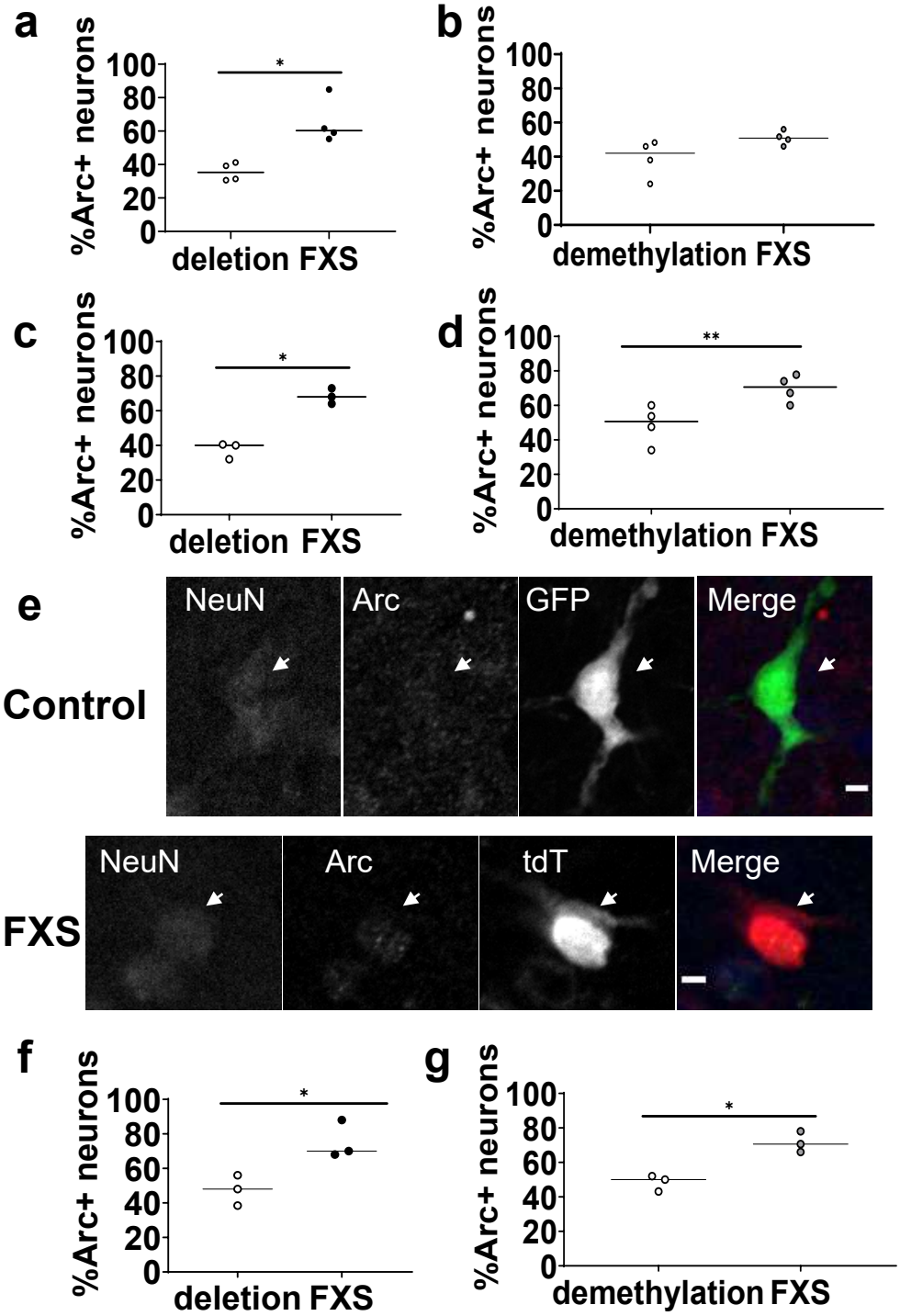

Figure 4: Transplanted FXS neurons show persistent increased Arc expression from 3 months PI. **a.** Percentage of isogenic control (deletion) and FXS Arc-positive neurons at 1 month PI. Paired t-test; N=4 animals, 36 to 78 neurons analyzed per animal per group. **b.** Percentage of isogenic control (demethylation) and FXS Arc-positive neurons at 1 month PI. Paired t-test; N=4 animals, 50 to 60 neurons analyzed per animal per group. **c.** Percentage of isogenic control (deletion) and FXS Arc-positive neurons at 3 months PI. Paired t-test; N=3 animals, 37 to 50 neurons analyzed per animal per group. **d.** Percentage of isogenic control (demethylation) and FXS Arc-positive neurons at 3 months PI. Paired t-test; N=4 animals, 50 to 61 neurons analyzed per animal per group. **e.** Confocal plane showing an isogenic control (demethylation) Arc-negative neuron and an FXS Arc-positive neuron at 3 months PI. White arrows indicate neuronal cell bodies. Scale bars represent 5 µm. **f.** Percentage of isogenic control (deletion) and FXS Arc-positive neurons at 6 months PI. Paired t-test; N=3 animals, 50 to 52 neurons analyzed per animal per group. **g.** Percentage of isogenic control (demethylation) and FXS Arc-positive neurons at 6 months PI. Paired t-test; N=3 animals, 50 to 51 neurons analyzed per animal per group. Neurons were defined as doublecortin-positive cells at 1 month post-injection (PI) and as NeuN-positive cells at 3 and 6 months PI. *: $p<0.05$; **: $p<0.01$. Thin horizontal bars in A-D, F, G indicate the mean.

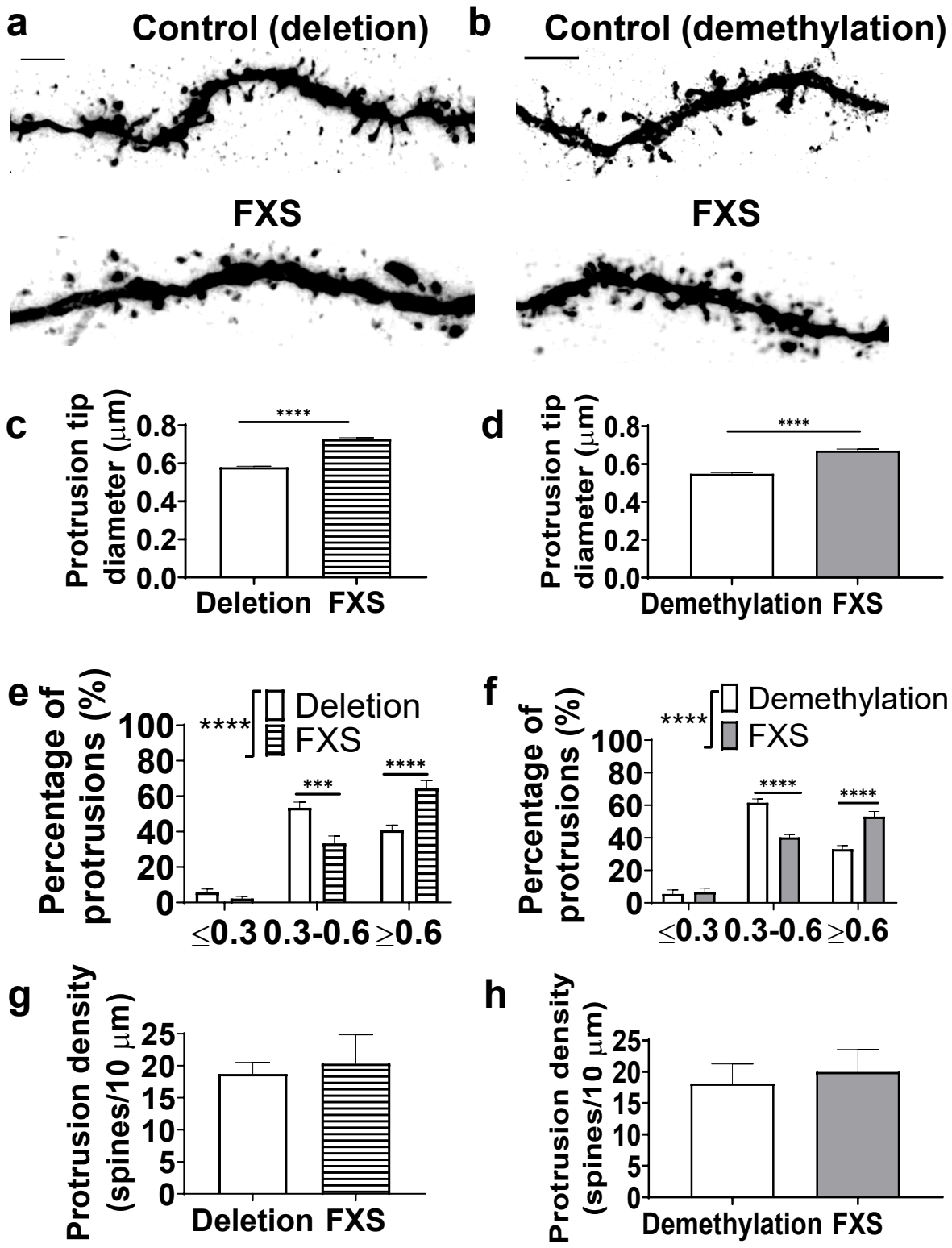

Figure 5: Wider dendritic protrusions in transplanted FXS striatal medium spiny neurons (MSNs) at 6-7 months post-injection. a. Representative 3D reconstructions of dendritic segments of control (deletion) (**upper panel**) and FXS (**lower panel**) MSNs. **b.** Representative 3D reconstructions of dendritic segments of control (demethylation) (**upper panel**) and FXS (**lower panel**) MSNs. Average tip diameter of dendritic protrusions of control and FXS MSNs from the deletion (**c**) and demethylation (**d**) pairs. Unpaired Mann-Whitney test; N=839 to 1742 protrusions from 6 to 11 MSNs per group. Percentage of protrusions with tip diameter inferior or equal to 0.3 µm (≤0.3), strictly comprised between 0.3 and 0.6 µm (0.3-0.6), or superior or equal to 0.6 µm (≥0.6) in control and FXS MSNs from the deletion (**e**) and demethylation (**f**) pairs. Mixed-effects model followed by Sidak's correction for multiple comparisons; N=6 to 11 MSNs per group. Average protrusion density of FXS and control MSNs from the deletion (**g**) and demethylation (**h**) pairs. *: p<0.05; **: p<0.01; ***: p<0.001; ****: p<0.0001. Bar heights and whiskers represent the mean +/- SEM. Scale bars represent 50 µm.

Figures

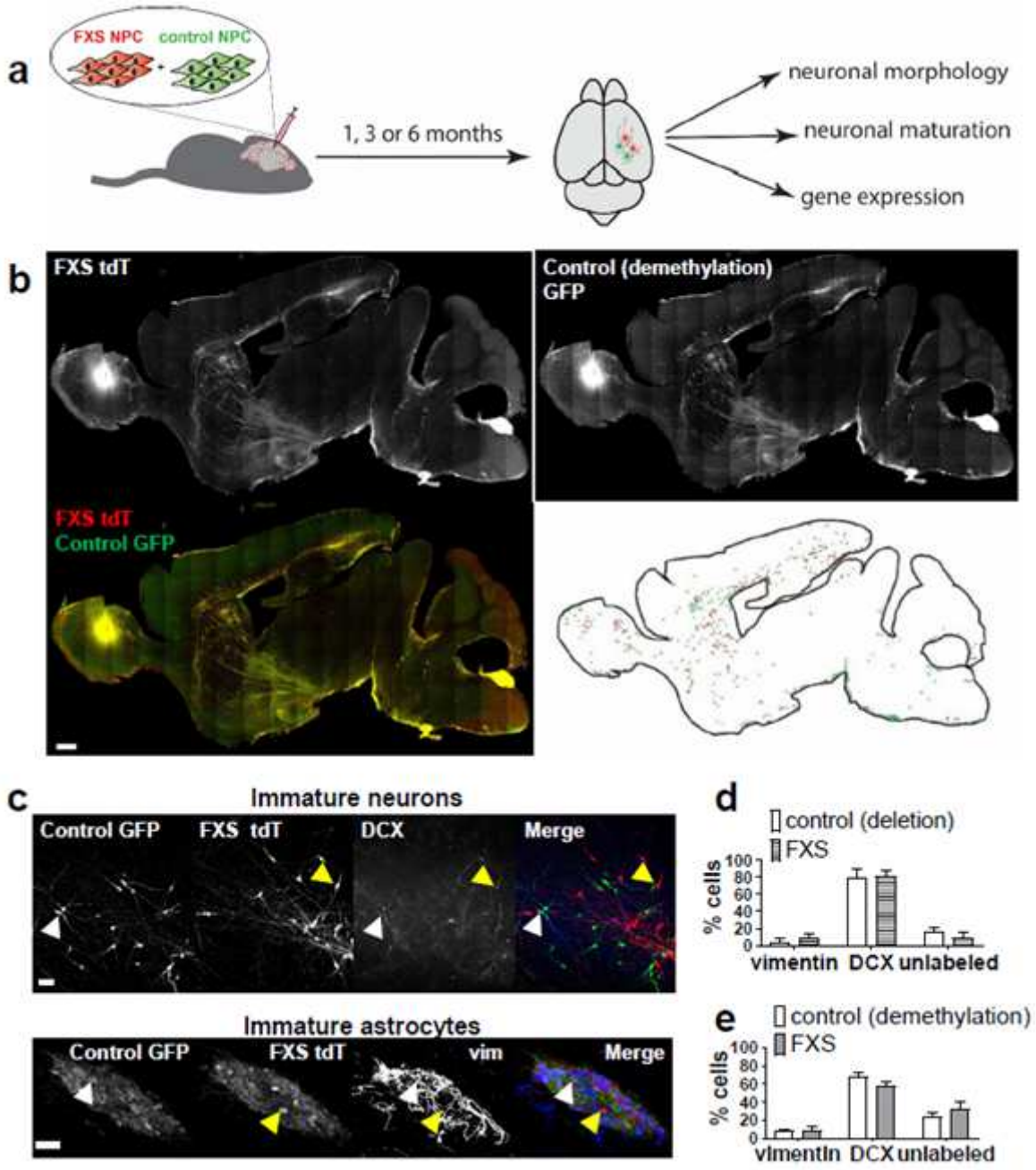

Figure 1

Transplanted hNPCs populate several areas of the brain and differentiate into neurons and astrocytes.

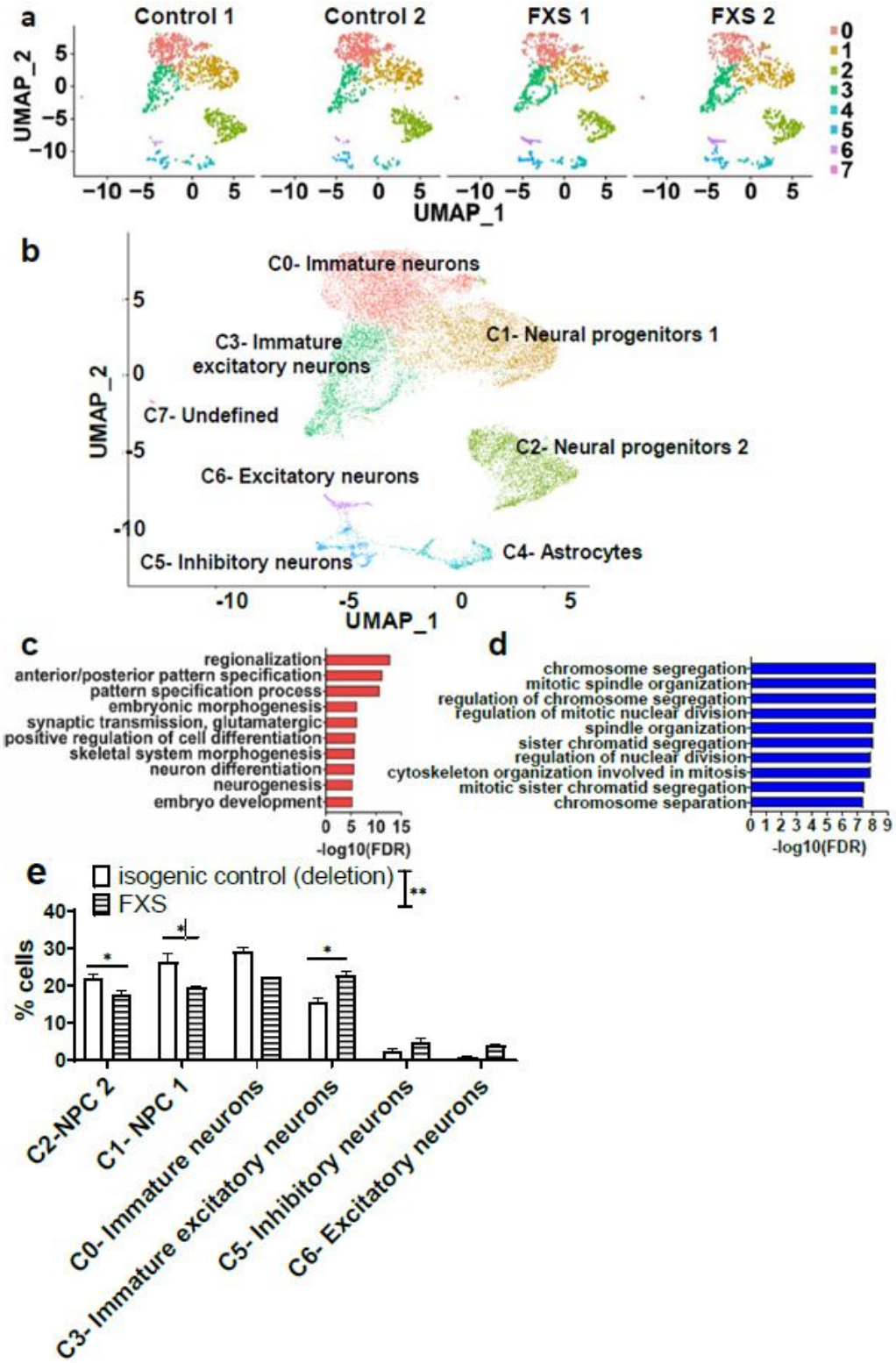

Figure 2

Single cell RNA sequencing of transplanted isogenic control and FXS neurons suggests increased maturation of FXS neurons and reveals upregulation of synaptic transmission, neuronal differentiation and neuronal development pathways in FXS neurons.

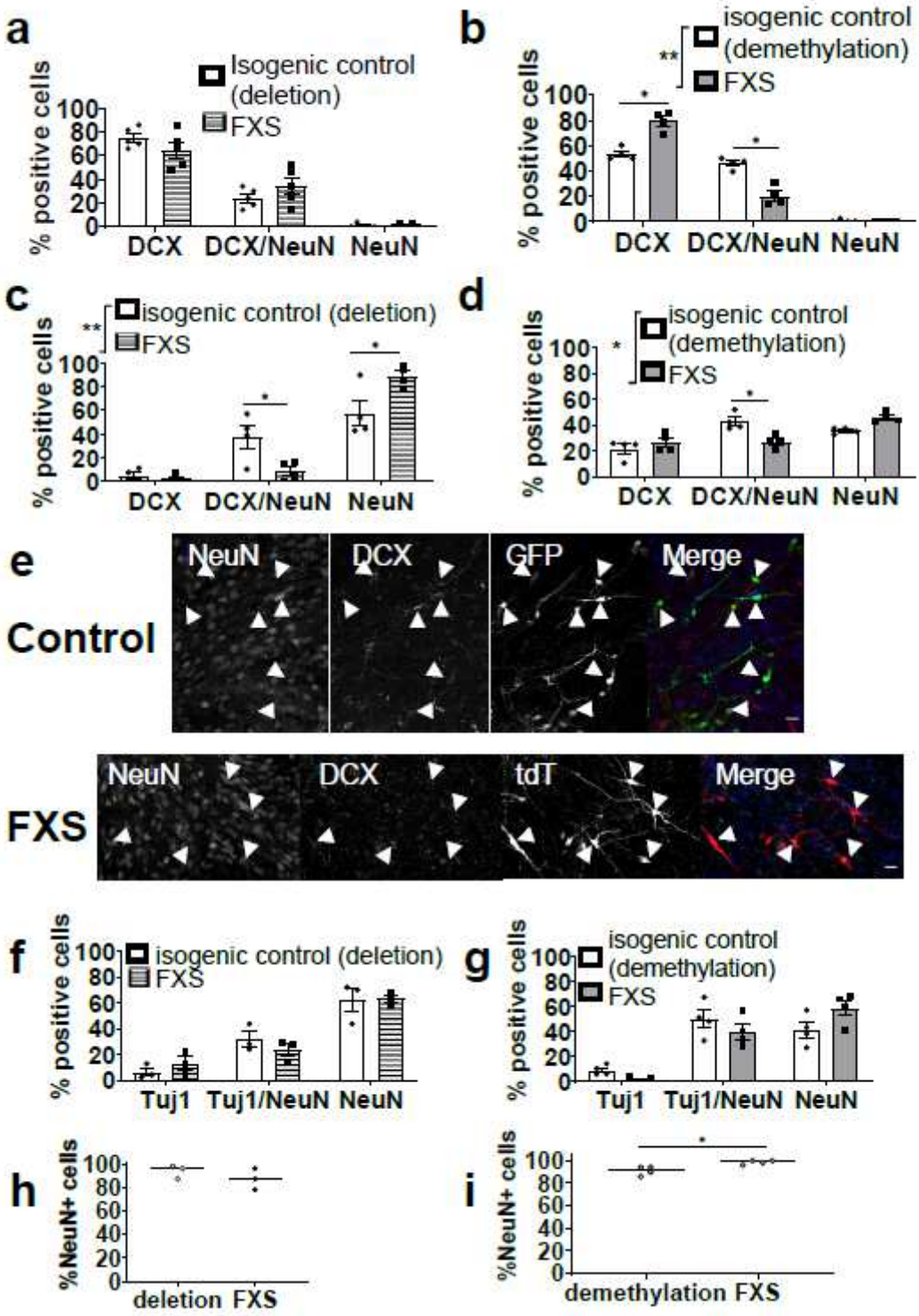

Figure 3

Transplanted FXS neurons mature faster than isogenic control. P

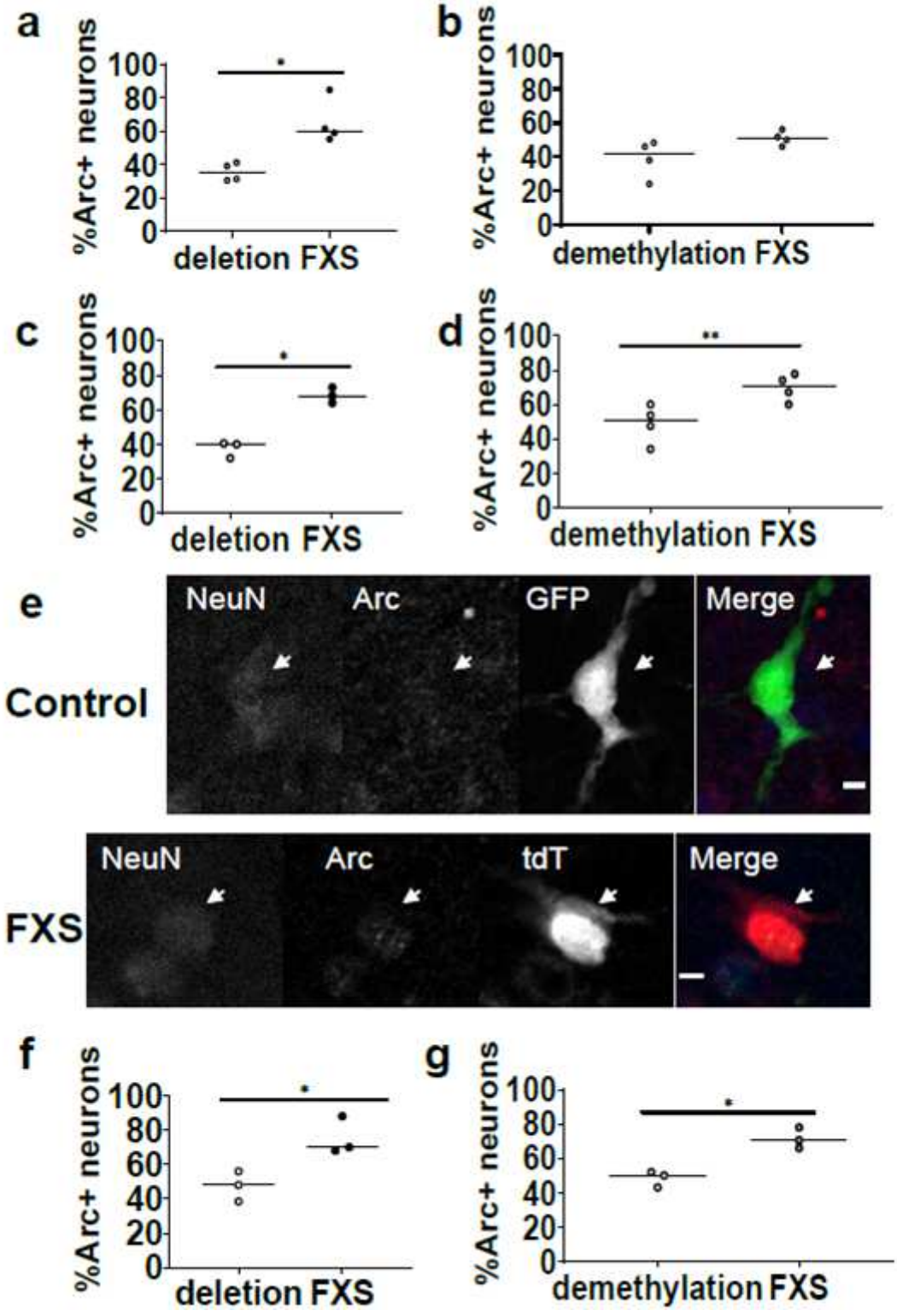

Figure 4

Transplanted FXS neurons show persistent increased Arc expression from 3 months PI.

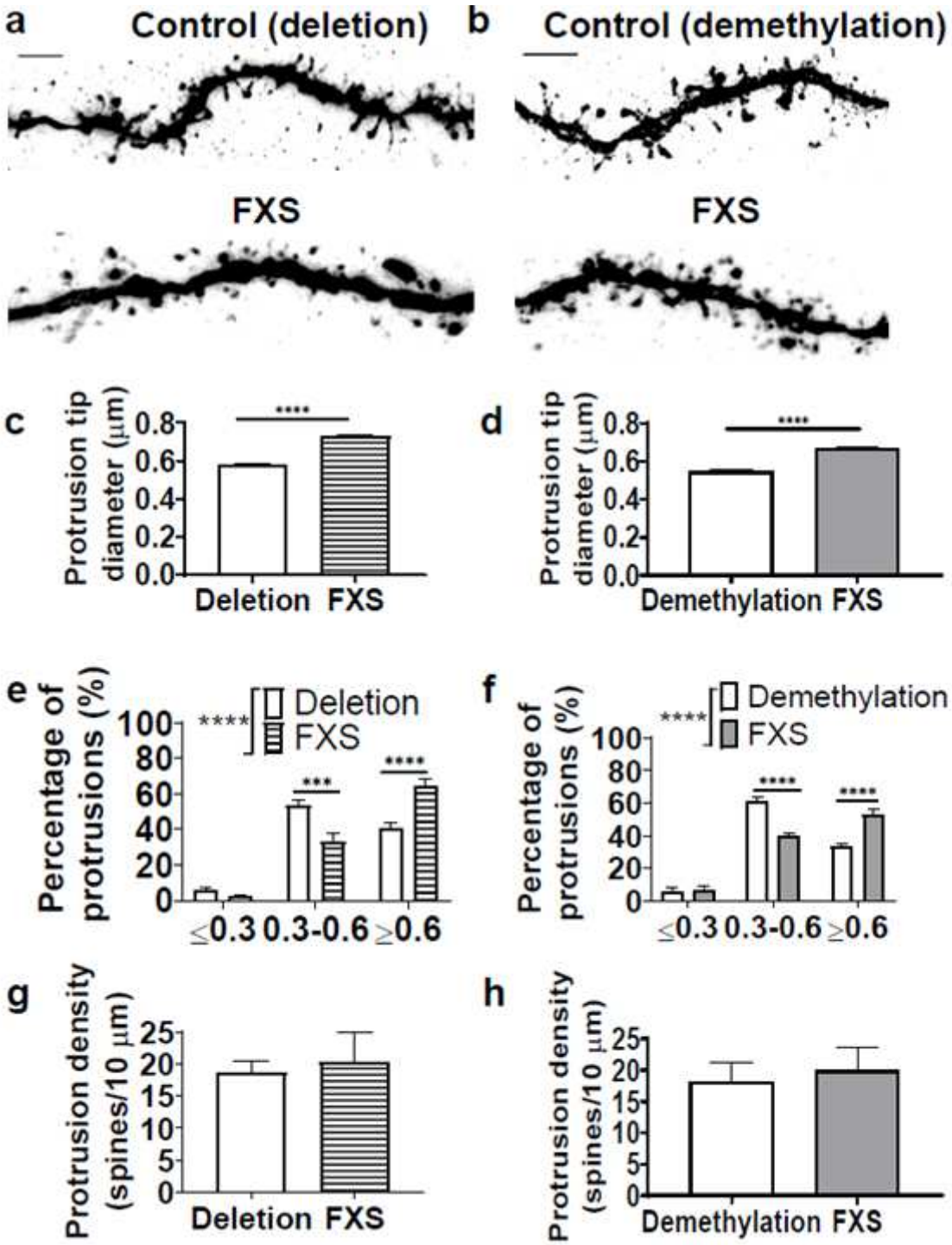

Figure 5

Wider dendritic protrusions intransplanted FXS striatal medium spiny neurons (MSNs) at 6-7 months post-injection.

Supplementary Files

This is a list of supplementary files associated with this preprint. Click to download.

- Supplmaterialandtables.pdf
- nrreportingsummary.pdf